

## Effect of Molybdenum and Silicon on Microstructural Evolution and Compressive Behaviour of Titanium Aluminide Based Alloys

Khalil Yacoubi<sup>1\*</sup>, Boutarek N<sup>1</sup> and Jahazi M<sup>2</sup><sup>1</sup>Department of Material Science, University of Sciences and Technology Houari Boumediene, Bab-Ezzouar, Algeria<sup>2</sup>Departement of Mechanical Engineering, School of Higher Technology, Quebec, Canada

### Abstract

Engineering grade intermetallic TiAl based alloys has been established as high performance alloys when compared to more traditional super alloys and other Ni based alloys thanks to excellent density/performance ratio.

**Objective:** This study aims to investigate new selected alloys compositions toward their use as structural materials for automotive and aeronautic industry.

**Methods:** Nominal compositions of Ti-45Al-5Nb-4V-0.5Mo-0.1Si, Ti-45Al-5Nb-4V-0.5Mo-0.5Si and Ti-45Al-5Nb-4V-0.3Si (at %) were casted and heat treated resulting in  $\gamma$  and  $\alpha/\gamma$  microstructure analyzed using scanning electron microscopy. To determine formability and mechanical behaviour at elevated temperature, hot compression tests were conducted at 1323 K and strain rate of  $0.05 \text{ s}^{-1}$  on deformation dilatometer DIL A/D 805.

**Results:** Microstructure imaging before and after deformation and stress strain curves were obtained. DRX (DXR) evidence was further explicated by exploitation of experiment data and calculation of dynamic recrystallization volume fraction of DRXed phases.

**Conclusion:** Results shows that mechanical performance of intermetallic TiAl alloys are microstructure depended. Casted Ti-45Al-5Nb-4V-0.5Mo-0.1Si alloy have promising mechanical performance and is subject to improvement toward application.

**Keywords:** Titanium aluminides; Intermetallics; TiAl; Microstructure; Electron microscopy; Hot compression test; Dynamic softening; Recrystallization; Compression behavior

### Introduction

TiAl based alloys represent an important class of alloys that exhibit a unique combination of physical and mechanical properties which include low density of  $3.7 \text{ g/cm}^3$ - $4.7 \text{ g/cm}^3$ , high elastic modulus, high creep resistance and good resistance against oxidation and corrosion which promote this binary alloy as a serious candidate to replace conventional structural materials in energy, automotive and aerospace industries [1-3]. However, after more than three decades of intensive research, very few TiAl based alloys did obtain a satisfactory level of maturity to be used for critical components in turbines and aircraft engines, mainly due to reduced toughness and low ductility at room temperature in comparison to those of conventional structural materials [4].

In order to improve mechanical properties and expand the application of TiAl based alloys, corresponding relations between mechanical properties and microstructure have been investigated widely, in the same context, a great number of studies have been made on the fracture mechanism of TiAl based alloys [5-11]. However, studies on the compressive behaviour are relatively rare. A large difference of deformability between tensile and compression tests was revealed, this variance is caused by the difference of stress and strain conditions. CT Liu showed that the yield strength was a function of the test temperature measured by compression tests at various test temperatures [11]. Pu, reported that the compression strength of Ti-Al-Cr-V alloy will increase at  $1170^\circ\text{C}$  when the strain rate changes from  $0.001 \text{ s}^{-1}$  to  $100 \text{ s}^{-1}$  [12].

Several approaches have been made to overcome the insufficiencies of TiAl based alloys. Among these methodologies, element alloying, which consist of introducing innovative elements into TiAl based alloy composition, has received considerable attention in the purpose of meet the optimal composition [13,14].

In this work, microstructure of heat treated, Ti45Al5Nb4V0.1Si and Ti45Al5Nb4V (Mo, Si (at % alloys were studied and hot deformation behaviours were discussed.

\*Corresponding author: Khalil Yacoubi, Department of Material Science, University of Sciences and Technology Houari Boumediene, Bab-Ezzouar, Algeria; E-mail: yacoubikhalil@gmail.com

Received: 08-August-2022, Manuscript No. JMSN-22-71445; Editor assigned: 11-August-2022, PreQC No. JMSN-22-71445 (PQ); Reviewed: 25-August-2022, QC No. JMSN-22-71445; Revised: 09-January-2023, Manuscript No. JMSN-22-71445 (R); Published: 16-January-2023, DOI: 10.4172/jmsn.100065

Citation: Yacoubi K, Boutarek N, Jahazi M (2023) Effect of Molybdenum and Silicon on Microstructural Evolution and Compressive Behaviour of Titanium Aluminide Based Alloys. J Mater Sci Nanomater 07:065.

Copyright: © 2023 Yacoubi K, et al. This is an open-access article distributed under the terms of the Creative Commons Attribution License, which permits unrestricted use, distribution, and reproduction in any medium, provided the original author and source are credited.

## Materials and Methods

The alloys with different compositions have been prepared from high purity elements (>99.8% purity). The prepared mixtures were arc melted with an induction furnace at least three times to ensure good homogeneity of the samples. The melting was conducted in a pure argon gas atmosphere.

As titanium and aluminium are very prone to oxygen contamination that may seriously affect the result of our elaboration, pure elements grits were cleaned in nitric acid (HNO<sub>3</sub>:1M), rinsed and dried, then

Alloy (% at)	Processing
Ti-45Al-5Nb-4V-0.3Si	Induction melting+Heat treatment 1200°C/16 h
Ti-45Al-5Nb-4V-0.5Mo-0.1Si	
Ti-45Al-5Nb-4V-0.5Mo-0.5Si	

**Table 1:** Chemical composition (% at) and processing of prepared alloys.

In order to perform metallographic observations, samples were sectioned, polished and observed by optical and Scanning Electron Microscopy (SEM). Alloys microstructures were studied using Olympus LEXT OLS4100 laser scanning microscope and Hitachi SU 8230 scanning electron microscope equipped with EDX (Energy Dispersive X-ray) analysis used to determine phase composition (semi quantitative).

In order to evaluate compressive behaviour, samples with 5 mm in diameter and 8 mm in height were cut from the prepared mass. Isothermal compression tests were conducted on a quenching dilatometer DIL 805A/D machine with argon atmosphere at temperature of 1323 K and strain rates of 0.05 s<sup>-1</sup>.

Before the compression, each Specimen was heated at a rate of 5 k/s and maintained for 5 min at target temperature for homogenization. The maximum strain obtained in the tests was 50%. Once compression ended, the specimens were quenched to room temperature immediately with cooling rate of 30 C/s. True stress curves were obtained.

## Results and Discussion

### Starting microstructures

Several studies have confirmed that initial microstructure of TiAl alloys, before deformation, has a significant role in final mechanical properties, following this aspect, microstructural assessment was carried out for the casted alloys [15-19].

weighed in stoichiometric proportions before introduction to the elaboration furnace.

Samples were heat treated after furnace elaboration, considering the affinity between titanium and aluminium with oxygen, the heat treatment was done under argon atmosphere. Samples were heated to 1200°C for 16 hours followed by slow cooling inside the furnace. Table 1 gives a summary of chemical composition and processing of prepared alloys.

Figure 1 expose the starting microstructure heat treated of Ti-45Al-5Nb-4V-0.3Si alloy. The material shows a nearly lamellar structure composed by large colonies of  $\gamma/\alpha_2$  along with coarse  $\gamma$  phase, Energy Dispersive Spectra (EDS) pointed at +1, +2 and +3 and listed in Table 2 summarize concentrations of addition elements in the alloy. Nb as addition element is homogeneously spread across both the  $\gamma/\alpha_2$  and the  $\gamma$  phase while vanadium and silicon preferentially positioned in the  $\gamma$  phase. XRD pattern where  $\gamma$ -TiAl and  $\alpha_2$ -Ti<sub>3</sub>Al phases are confirmed with the identification of  $\beta$  phase in significant less extend.

Microstructure of second alloy Ti-45Al-5Nb-4V-0.5Mo-0.1Si is depicted (Figures 2 and 3). Similarly to previous material, the microstructure exhibit two main regions. XRD analysis, presented in Figure 4, confirmed composition is mainly  $\gamma/\alpha_2$  along with  $\gamma$  phase and  $\beta$  phase. In this case, the addition of molybdenum and reduction of silicon content, comparatively to previous alloy, had qualitatively enlarged lamellar  $\gamma/\alpha_2$  and decreased  $\gamma$  phase ratio. It is generally admitted that Mo addition has a positive impact on ductility [20]. EDS results are summarized in Table 2.

This depict microstructure of Ti-45Al-5Nb-4V-0.5Mo-0.5Si, elevation of silicon content to 0.5% (at %) comparatively to 0.1% (at %) in previous second alloy impacted initial, heat treated microstructure with formation of long precipitation chain, EDS analysis summarized revealed high silicon concentration and confirmed precipitation nature of the ribbons that have subsisted to the heat treatment.

Alloy		Ti (at %)	Al (at %)	Nb (at %)	V (at %)	Si (at %)	Mo (at %)
Ti-45Al-5Nb-4V-0.3Si	+1	46.97	44.85	7.58	0.52	0.09	-
	+2	49.89	35.73	8.80	4.27	0.79	-
	+3	48.26	43.30	7.18	1.10	0.12	-

Ti-45Al-5Nb-4V-0.5Mo-0.1Si	+1	46.37	36.39	10.49	4.59	0.92	0.75
	+2	46.48	35.73	8.18	1.24	0.15	-
	+3	46.58	35.90	10.47	4.87	1.01	1.15
Ti-45Al-5Nb-4V-0.5Mo-0.5Si	+1	44.89	24.17	9.96	2.91	18.08	-
	+2	46.83	35.73	7.70	0.98	0.55	-
	+3	48.30	35.95	10.05	4.56	0.99	0.14

**Table 2:** Results of energy dispersive spectra of the alloys.

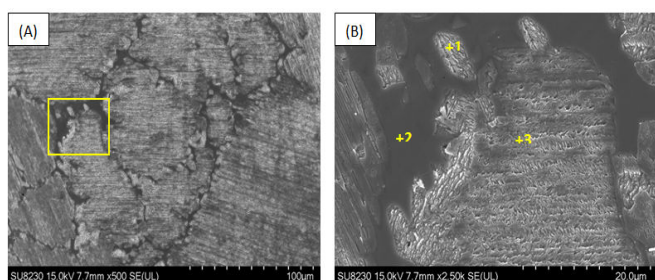


**Figure 1:** Scanning Electron micrographs (SE mode) of Ti-45Al-5Nb-4V-0.3Si alloy.

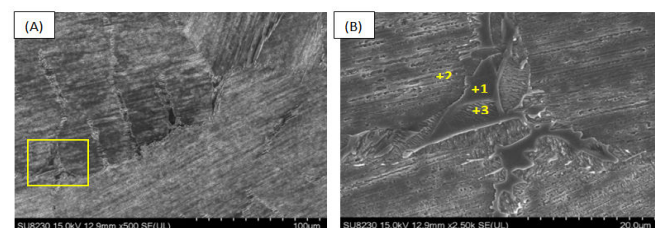


**Figure 2:** Scanning Electron micrographs (SE mode) of Ti-45Al-5Nb-4V-0.5Mo-0.1Si alloy.

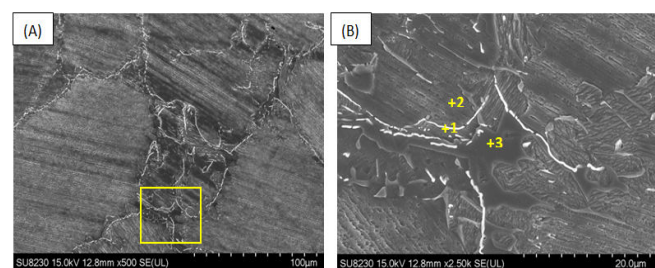


**Figure 3:** Scanning Electron micrographs (SE mode) of Ti-45Al-5Nb-4V-0.5Mo-0.5Si alloy.

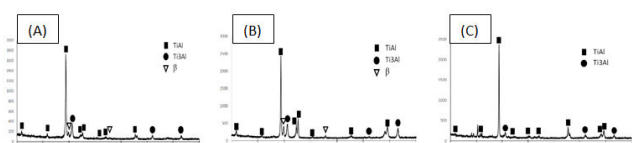


**Figure 4:** XRD patterns of (a). Ti-45Al-5Nb-4V-0.3Si, (b). Ti-45Al-5Nb-4V-0.5Mo-0.1Si, (c). Ti-45Al-5Nb-4V-0.5Mo-0.5Si.

## Deformation behaviour

**Compression properties:** The true stress strain curves of various TiAl based alloys less than 1323 K and  $0.05 \text{ s}^{-1}$  are illustrated in Figure 5. It can be seen that most of flow stress trends increase to peak value before decreasing until a steady state is reached. The Ti-45Al-5Nb-4V (Mo, Si) samples deformed at 1323 K and  $0.05 \text{ s}^{-1}$  exhibit greater effect of DRX softening where Ti-45Al-Ti-45Al-5Nb-4V-0.3Si specimen shows more steady state curves.

It is well known that deformation mechanisms at hot temperatures rely on dynamic softening and work hardening processes. The hot compression process can be separated into three stages: At initial stage of deformation, flow stress increases rapidly due to increasing density of dislocations till a peak stress is reached; at this stage, work hardening exceeds dynamic softening which generates the sharply increasing tendency. Successively, the deformation energy accumulated with the growth of deformation strain will offsets the work hardening and brings forward dynamic softening mechanism which diminishes the dislocation density, inducing decrease in true stress. This decreasing tendency at this stage is characteristic of dynamic recrystallization over dynamic recovery during deformation [21,22]. When the work hardening and dynamic softening reach a dynamic equilibrium, the dislocation density remains relatively constant, and a steady state flow stress is obtained as shown on the curves.

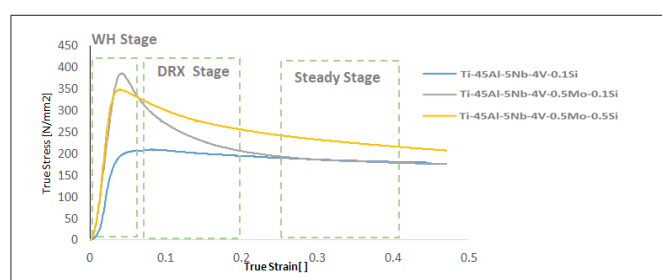


**Figure 5:** True stress true strain curves of tested alloys under 1323 K and  $0.05 \text{ s}^{-1}$ , WH stage refers to work hardening stage, DRX stage refers to dynamic recrystallization stage.

As the true stress of the alloys increases with the increase in the strain rate in the first work hardening stage. The alloys exhibit significant difference in the ultimate true stress, it is observed that Ti-45Al-5Nb-4V (Mo, Si) alloys shows higher strength than Ti-45Al-5Nb-4V-0.3Si. Because the alloys have similar overall starting microstructures, the differences in the compression behaviour could be mainly due to the difference in solid solution of alloying elements such as Mo and V and difference in dislocation density.

**Microstructures after deformation:** This shows microstructures of hot compressed alloys, deformed at 1323 K and  $0.05 \text{ s}^{-1}$ .

The stressed materials exhibit deformed microstructure and heavily elongated  $\gamma/\alpha_2$  colonies in direction perpendicular to force application in all three alloys.

In Figure 6, Ti-45Al-5Nb-4V-0.3Si lamellar colonies are shown elongated perpendicularly to compression force. Different dislocation movement and slips systems were activated to process the deformation resulting twisting and bending in multiples orientations. The lack of clear dynamic recrystallisation manifestation suggests that compression at 1323 K and  $0.05 \text{ s}^{-1}$  didn't provide sufficient energy to reach recrystallization stage.

With addition of molybdenum, Ti-45Al-5Nb-4V-0.5Mo-0.1Si alloy shows, in Figure 7, deformed microstructure with evidence of dynamic recrystallization. Both  $\alpha^2$  and  $\gamma$  phases undergo driving force for recrystallization resulting from the energy of deformation [23]. Recrystallization driving force are dependent to deformation subjected, therefore, in  $\gamma/\alpha_2$  colonies with higher deformation (*i.e.* higher forces) dynamic recrystallization took place and fine DXR grains are formed [24,25].

Figure 8 show microstructure of Ti-45Al-5Nb-4V-0.5Mo-0.5Si after hot compression test. The long precipitate chains were fractured into small coarse grains. Similarly to previous alloy, dynamic recrystallization process was identified with appearance of new fine DXR grains. When recrystallization driving force are strong enough, the precipitates act as nucleation sites for recrystallization and enhance microstructural refinement [26,27].

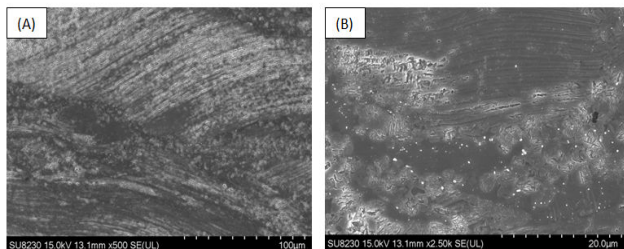


**Figure 6:** Scanning electron micrographs of Ti-45Al-5Nb-4V-0.3Si alloy after the compression test.

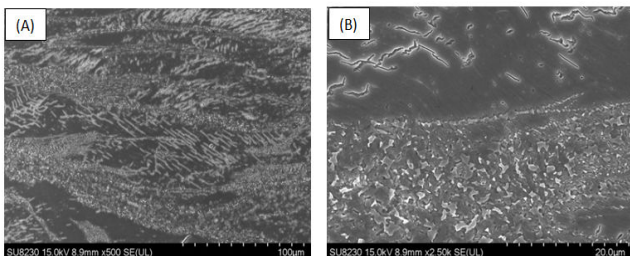


**Figure 7:** Scanning electron micrographs of Ti-45Al-5Nb-4V-0.5Mo-0.1Si alloy after the compression test.

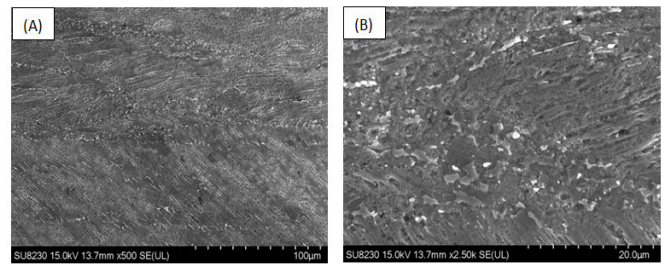


**Figure 8:** Scanning electron micrographs of Ti-45Al-5Nb-4V-0.5Mo-0.5Si alloy after the compression test.

**Dynamic recrystallization volume fraction:** Dynamic Recrystallization (DRX) commence with the increase of dislocation density which is a thermally activated process [28]. With further plastic deformation heat, more potential DRXed nucleus will form resulting in new recrystallized grains [29]. DRX behavior can be further examined with the calculation of the recrystallization volume fraction using the modified Avrami type equation:

$$X_{DRX} = 1 - \exp \left[ -k \left( \frac{\epsilon - \epsilon_c}{\epsilon^*} \right)^n \right] \quad (1)$$

Where  $X_{DRX}$  is the volume fraction of DRXed grains,  $\epsilon^*$  is the strain for maximum softening rate;  $\epsilon_c$  is the critical strain and  $k$  and  $n$  are material constants [30].

From equation (1) above, it is shown that critical strain is important in calculation and prediction of microstructural DRX evolution. Several mathematical models have been proposed by researchers to spot the critical condition for the commencement of dynamic recrystallization using flow stress curves. In this work, the work hardening rate ( $\theta = \partial\sigma/\partial\epsilon$ ) was calculated [31,32].

The  $\theta$ - $\sigma$  curve of Ti-45Al-5Nb-4V-0.5Mo-0.1Si alloy under 1323 K and strain rate of  $0.05 \text{ s}^{-1}$  is shown in Figure 9. The work hardening curve show typically four stages: stage I begins from initial stress to the critical stress ( $\sigma_c$ ), where the value of  $\theta$  decreases sharply, and the inflection point on the  $\theta$ - $\sigma$  curve demonstrates the onset of DRX. Stage II covers the transition between the DRX commencements (corresponding to  $\sigma_c$ ) to the peak stress, where  $\theta$  hits zero. Stage III is where  $\theta$  reaches the lowest value indicates maximum softening and DRX prevalence region, it begins at  $\sigma_p$  and ends at  $\sigma^*$ . Last stage IV is where equilibrium between work hardening and DRX softening occurs and  $\theta=0$  [33, 34].

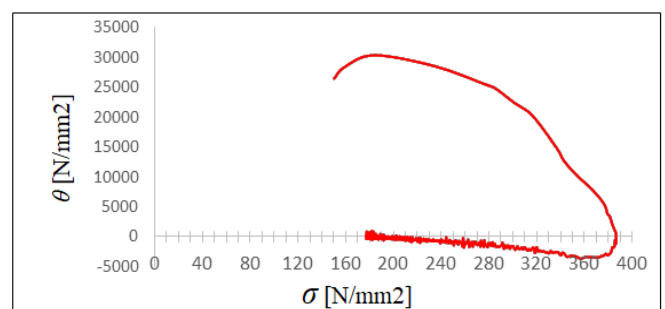


**Figure 9:** Hardening rate curve of Ti-45Al-5Nb-4V-0.5Mo-0.1Si alloy under 1323K and strain rate of  $0.05 \text{ s}^{-1}$ .

J Liu proposed that flow stress function of DRX can be expressed as:

$$X_{DRX} = \frac{\sigma - \sigma_P}{\sigma_S - \sigma_P} \quad (2)$$

Where  $\sigma_p$  is the peak stress and  $\sigma_s$  is the steady state stress.

Based on equation (1), the below is obtained:

$$\ln[-\ln(1 - X_{DRX})] = n \ln\left[\frac{\varepsilon - \varepsilon_c}{\varepsilon^*}\right] + \ln k \quad (3)$$

With the condition of 1323 K and  $0.05 \text{ s}^{-1}$ , the relationship between  $\ln[-\ln(1 - X_{DRX})]$  and  $\ln[(\varepsilon - \varepsilon_c)/\varepsilon^*]$  is plotted and the values of n and k are determined to be 1.021 and 0.229, respectively.

Following the findings, volume fraction of Ti-45Al-5Nb-4V-0.5Mo-0.1Si alloy in testing conditions can be expressed as:

$$X_{DRX} = 1 - \exp\left[-0.795 \left(\frac{\varepsilon - 0.018}{0.030}\right)^{2.30}\right] \quad (4)$$

DRX volume fraction is shown in Figure 10 where it can be seen that the dynamic recrystallization will not occur at strain less than the critical strain  $\varepsilon_c$ . The volume fraction of DRXed grains increases as the strain increases.

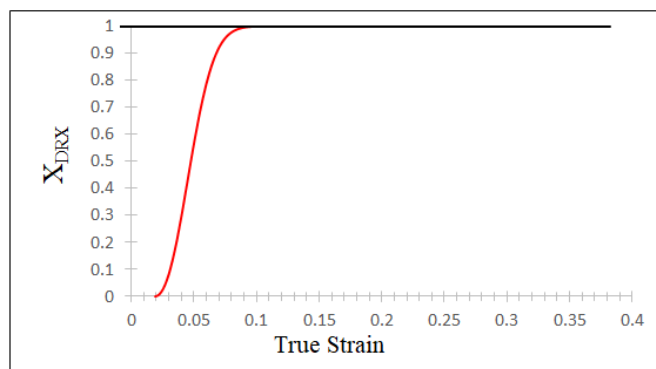


**Figure 10:** DRX volume fraction curve of Ti-45Al-5Nb-4V-0.5Mo-0.1Si alloy under 1323 K and strain rate of  $0.05 \text{ s}^{-1}$ .

## Conclusion

In an effort of assessing addition element impact on mechanical proprieties in intermetallic TiAl based alloys and toward mechanical performance enhancement, alloys with nominal composition of Ti-45Al-5Nb-4V-0.5Mo-0.1Si, Ti-45Al-5Nb-4V-0.5Mo-0.5Si, and Ti-45Al-5Nb-4V-0.3Si (at %) were casted, heat treated, the obtained materials were subsequently mechanically assessed using hot compression test at 1323 K and strain rate of  $0.05 \text{ s}^{-1}$ . The resulting

microstructures were further evaluated through microstructural analysis.

The following summarizes key finding of the study:

- The nearly lamellar microstructure exhibits typical compression behaviour of intermetallic TiAl alloys with dynamic flow and softening features seen on the true stress true strain curves. Under hot compression of 1323 K and strain rate of  $0.05 \text{ s}^{-1}$ , dynamic recrystallization behavior was not obviously reached for Ti-45Al-5Nb-4V-0.3Si suggesting that deformation activation energy of the alloy is larger than the other casted alloys. This observation further indicates that Ti-45Al-5Nb-4V-0.3Si alloy tend to have low hot workability when compared to Ti-45Al-5Nb-4V (Mo, Si) tested alloys for which dynamic recrystallization was more obvious.
- Molybdenum addition at 0.5% (at %) improve general compression behavior. The Ti-45Al-5Nb-4V-0.5Mo-0.1Si alloy exhibit highest strength, flow stress decreases significantly toward steady state with increasing strain, indicating best hot workability behaviour.

## References

1. Dimiduk DM (1999) Gamma titanium aluminide alloys-An assessment within the competition of aerospace structural materials. Mater Sci Eng A 263: 281-288.
2. Loria EA (2000) Gamma titanium aluminides as prospective structural materials. Intermetallics 8: 1339-1345.
3. Clemens H, Smarsly W (2011) Light weight intermetallic titanium aluminides-status of research and development. Adv Mat Res 278: 551-556.
4. Leyens C, Peters M (2005) Titanium and titanium alloys fundamentals and applications. John Wiley and Sons, 77-79.
5. Zhang DY, Li HZ, Liang XP, Wei ZW, Liu Y (2014) Microstructure characteristic for high temperature deformation of powder metallurgy Ti-47Al-2Cr-0.2Mo alloy. Mater Des 59: 415-420.
6. Thomass S, Michael MM, Francisca S, Thomas, Boryana R, et al. (2015) Carbon distribution in multi-phase  $\gamma$ -TiAl based alloys and its influence on mechanical properties and phase formation. Acta Mater 94: 205-213.
7. Yokoshima S, Yamaguchi M (1996) Fracture behavior and toughness of PST crystals of TiAl. Acta Mater 44: 873-883.
8. Rogers NJ, Crofts PD, Jones IP, Bowen P (1995) Microstructure toughness relationships in fully lamellar  $\gamma$ -based titanium aluminides. Mater Sci Eng A 192: 379-386.
9. Chan KS, Kim YW (1992) Influence of microstructure on crack tip micromechanics and fracture behaviors of a two phase TiAl alloy. Metall Trans A 23: 1663-1677.
10. Chan KS (2000) The fracture resistance of a binary TiAl alloy Metall. Mater Trans A 31A : 71-80.
11. Liu CT, Schneibel JH, Maziasz PJ (1996) Tensile properties and fracture toughness of TiAl alloys with controlled microstructures. Intermetallics 4: 429-440.
12. Pu ZJ, Wu KH, Shi J, Zou D (1995) Development of constitutive relationships for the hot deformation of boron microalloying TiAl-Cr-V alloys. Mater Sci Eng A 192: 780-787.
13. Wang NJ, Zhu J, Wu JS, Du XW (2002) Effects of alloying elements on creep of TiAl alloys with a fine lamellar structure. Acta Mater 50: 1307-1318.
14. Brotzu A, Felli F, Pilone D (2014) Effect of alloying elements on the behaviour of TiAl based alloys. Intermetallics 54: 176-180.
15. Schwaighofer E, Clemens H, Lindemann J, Stark A, Mayer S (2014) Hot-working behavior of an advanced intermetallic multiphase TiAl based alloy. Mater Sci Eng 614: 297-310.

16. Erdely P, Staron P, Maawad E, Schell N, Clemens H, et al. (2018) Lattice and phase strain evolution during tensile loading of an intermetallic, multiphase TiAl based alloy. *Acta Mater* 158: 193-205.
17. Kim YW (1998) Strength and ductility in TiAl alloys. *Intermetallics* 6: 623-628.
18. Tian S, Lv X, Yu H, Wang Q, Jiao Z, et al. (2016) Creep behavior and deformation feature of TiAl-Nb alloy with various states at high temperature. *Mater Sci Eng A* 651: 490-498.
19. Dimiduk D (1999) Gamma titanium aluminide alloys-An assessment within the competition of aerospace structural materials. *Mater Sci Eng A* 263: 281-288.
20. Appel F, Wagner R (1998) Microstructure and deformation of two-phase  $\gamma$ -titanium aluminides. *Mater Sci Eng* 22: 178-268.
21. Sakai T (1995) Dynamic recrystallization microstructures under hot working conditions. *J Mater Process Technol* 53: 349-361.
22. Ding R, Guo ZX (2001) Coupled quantitative simulation of microstructural evolution and plastic flow during dynamic recrystallization. *Acta Mater* 49: 3163-3317.
23. Schmoelzer T, Liss KD, Kirchlechner C, Mayer S, Stark A, et al. (2013) An *in-situ* high-energy X-ray diffraction study on the hot-deformation behavior of  $\beta$  phase containing TiAl alloy. *Intermetallics* 39: 25-33.
24. Imayev R, Oehring M, Appel F (2007) Alloy design concepts for refined gamma titanium aluminide based alloys. *Intermetallics* 15: 451-460.
25. Zhang S, Zhang C, Du Z, Hou Z, Lin P, et al. (2016) Deformation behavior of high Nb containing TiAl based alloy in  $\alpha+\gamma$  two phase field region. *Mater Des* 90: 225-229.
26. Chladil HF, Clemens H, Otto A, Güther V, Kremmer S, et al. (2006) Characterization of a  $\beta$ -solidifying  $\gamma$ -TiAl base alloy. *BHM Berg Huttenmann* 151: 356-36.
27. Li J, Liu Y, Wang Y, Liu B, He Y (2014) Dynamic recrystallization behavior of an as-cast TiAl alloy during hot compression. *Mater Charact* 97: 169-177.
28. Werner R, Schwaighofer E, Schloffer M, Clemens H, Lindemann J, et al. (2016) Constitutive analysis and microstructure evolution of the high-temperature deformation behavior of an advanced intermetallic multiphase  $\gamma$ -TiAl-based alloy. *Adv Mater Res* 922: 807-812.
29. Wilson PW (2013) Recent developments in the study of recrystallization. *InTech*.
30. Lv BJ, Peng J, Shi DW, Tang AT, Pan FS (2013) Constitutive modeling of dynamic recrystallization kinetics and processing maps of Mg-2.0Zn-0.3Zr alloy based on true stress strain curves. *Mater Sci Eng A* 560: 727-733.
31. Liu YH, Ning YQ, Yao ZK, Li H, Miao XP, et al. (2016) Plastic deformation and dynamic recrystallization of a powder metallurgical nickel-based superalloy. *J Alloys Compd* 675: 73-80.
32. Liu HJ, Ryan ND (2002) Constitutive analysis in hot working. *Mater Sci Eng* 322: 43-63.
33. Shaban M, Eghbali B (2010) Determination of critical conditions for dynamic recrystallization of a microalloyed steel. *Mater Sci Eng A* 527: 4320-4325.
34. Liu J, Cui Z, Ruan L (2011) A new kinetics model of dynamic recrystallization for magnesium alloy AZ31B. *Mater Sci Eng A* 529: 300-310.